Article │ Received 5 November 2024; Accepted 7 February 2025; Published 27 February 2025
https://doi.org/10.55092/am20250006

Study on the detection and suppression methods of carbon laying defects in auto fiber placement (AFP) process

Yixuan Xie, Zhiqiang Liu*, Yinqi Li and Yueyue Zong

School of Mechanical Engineering, Jiangsu University of Science and Technology, Zhenjiang, China

* Correspondence author; E-mail: zhiqiangliu@just.edu.cn.

Highlights:

- Thermal imaging was used to identify and locate defects in the process of carbon fiber laying.
- The defects are suppressed by temperature control.
- The control model of temperature suppression defects is completed.

Abstract: This paper proposes an optimal control strategy for process parameters aimed at addressing layup defects, achieving defect recognition and localization, and maintaining temperature stability on the actual layup surface. Infrared thermography is employed to identify defects during the carbon fiber layup process, and by integrating path control, the identification and localization of defects during the layup are effectively achieved. The minimum edge detection rate on both sides of a single layer reaches 94.3%, and the interlayer gap measurement is below 10%. Considering that temperature instability on the layup surface can lead to defects, a dynamic temperature control model has been established, and the infrared lamp's temperature rise coefficient is determined, reducing defects caused by temperature fluctuations during the layup process. The results indicate that infrared thermography technology is feasible for the detection and reduction of defects in CFRP composites.

Keywords: infrared thermography; laying defects; constant temperature control; automated fiber placement; damage localization

1. Introduction

Carbon fiber composites are high-performance materials composed of two or more materials with different properties. Through various processing methods, these materials are transformed into composites with specific mechanical properties. They exhibit high specific strength and modulus, effectively withstand high temperatures and fatigue, and demonstrate significant thermal stability [1]. In recent years, due to the excellent material properties including light weight, high specific strength, high temperature resistance, corrosion resistance, and strong design ability [2–6], carbon fiber composite materials have been widely used in the aircraft body, high-speed train, subway body, and bogie [7–8].

The weight ratio of carbon fiber composite materials used has become one of the important indicators of the advanced degree of high-end equipment. However, carbon fiber composite structures may appear defects during the complex manufacturing process, delamination and fatigue cracks may occur during long-term service resulting from external impact or fatigue loading, causing performance degradation and threatening operational safety. Therefore, it is of great significance to study structural health monitoring and damage detection techniques of composite structures [9–11].

The basic types of commonly used non-destructive testing (NDT) defect detection techniques include acoustic emission, ultrasonic testing, eddy current testing, infrared thermal imaging, terahertz testing, and X-ray computed tomography [12]. Acoustic emission is expensive but offers high detection speed, real-time health monitoring, and high sensitivity. It requires the entire structure of the sample to allow the propagation of stress waves. Ultrasonic testing has a fast detection speed, but data processing takes time to achieve accurate results, and it is difficult to detect defects near the probe. It is suitable for on-site inspection with portable equipment. Eddy current testing is relatively inexpensive and has a high detection speed, capable of detecting small defects, damage, and complex structures. However, it is limited to conductive composites and cannot detect surface defects. Infrared thermal imaging is moderately priced, with high detection speed, real-time and full-field defect detection, and is safe and easy to operate. However, it generally can only detect surface defects. Terahertz testing requires complex and expensive equipment and has a slow speed but high accuracy. X-ray computed tomography is expensive, slow, with limited testing range and harmful radiation to humans, but it is suitable for various materials with high spatial resolution and sensitivity. Broberg, in his work [13], pointed out that the advantage of laser heating of the test material using a point method in thermal imaging studies is the ease of controlling the size of the heating area and the duration of the heating time. Broberg also suggested that guiding the laser through fiber optic transmission makes directing the laser easier. Keo *et al.* [14], compares heating with a long laser pulse with optical lock-in thermography (heating with halogen lamps) as the main advantage of laser heating and considers unidirectional beam char-acteristics, which allows the sample to be heated in a specific position and area. The benen of laser heating is that it generates spherical heat flow in the test material, enabling the detection of material voids in any direction, as shown by Schlichting *et al.* [15] and Roemer *et al.* [16]. In a paper by Pech-May *et al.* [17], the advantage of laser heating was stated to be the measurement speed. Fedala *et al.* [18] noted the potential of laser lock-in thermography for locating cracks in specific areas of metal samples, which is difficult to achieve with traditional NDT methods (eddy current, ultrasonic). Thus, infrared thermal imaging is favored for its lower cost, ease of operation, and wide scanning range.

The suppression of interlayer defects during placement is primarily achieved by optimizing placement process parameters and coordinating the interlayer adhesion performance of viscoplastic prepreg, thereby improving interlayer bonding performance and suppressing defects such as voids, delamination, and fiber bridging. The key to suppressing interlayer defects lies in controlling placement pressure, placement temperature, and placement rate. Luckaszewicz [19], through experimental and theoretical analysis, examined the effects of prepreg interface and forming process on defects during placement forming, and proposed an optimization model for the process conditions of high-speed prepreg automated placement forming. Hulcher *et al.* [20] used peel tests to study the effects of placement pressure and applied the response surface methodology to obtain a quantitative relationship between placement pressure and the quality of placed components. Aized *et al.* [21] established a method

for evaluating placement quality based on the interlayer adhesion between the prepreg and the placement mold. In this context, this paper studies the methods for defect identification and localization during the placement process based on thermal imaging.

In view of the above considerations, this paper firstly set the defects during the automatic laying of the carbon fiber manually, and locate them through the detection and analysis of the thermal imager. Compared to other detection methods, the price is appropriate, the detection speed is high, the real-time detection is safe and easy to operate. Then, according to the influence of temperature on defects during the laying process, a dynamic constant temperature control model is proposed. The experimental data and theoretical model are used to complete the research on temperature control, so as to realize the suppression of defects in the laying process.

2. Identification of defects methodology using the thermal imaging

2.1. Experimental setup and procedures of identification defects

2.1.1. Experimental set up

Infrared thermal imaging is a non-contact technology with the characteristics of wide measurement range, fast measurement speed and high acquisition frequency, which can record the temperature field of composite materials [22].A typical infrared thermal imaging system contains an infrared radiometer, with or without energy, synchronization, and control panel, display software [23]. The application of infrared thermal imaging technology can be divided into passive thermal imaging and active thermal imaging. In passive thermal imaging, thermal radiation is emitted directly from the surface of the test object [24]. In active thermal imaging, a heating or cooling flow is generated and propagated to the test object, and the thermal response is detected according to the Stefan-Bolzmann law [25]. Infrared thermal imaging technology has the capability to identify various types of defects that may arise during the automated deposition of carbon fibers through the analysis of energy dissipation. Consequently, this study introduces a method for monitoring the placement process, which relies on detecting temperature variances that occur during the layering process. Additionally, a new monitoring system utilizing an infrared camera is proposed. Through the integration of the placement trajectory's spatial position, coordinate positioning, and specific abnormal temperature readings, it becomes feasible to detect and pinpoint placement defects.

The defect detection system for the patching process is shown in Figure 1 and includes a FLIR A615 infrared thermography camera, a computer, carbon fiber patching equipment, and a patching mold. To simplify the defect identification experiment, a flat mold is used for the placement of the laminated board. The infrared camera is strategically positioned slightly above the mold, behind the placement direction, with the mold placed on an aluminum platform. The heating device is located at the bottom of the placement head, positioned in front of the compaction roller. During the placement process, the infrared camera detects temperature changes in the cooler areas of the compaction points. The computer interface visually represents these temperature differences, indicating that the maximum temperature difference occurs just behind the compaction roller. In the case of gaps of specific sizes, surface radiation can be observed through these gaps, leading to localized peak temperatures. Conversely, in overlapping situations, the amount of placed material is effectively doubled, resulting in the lowest local temperature.

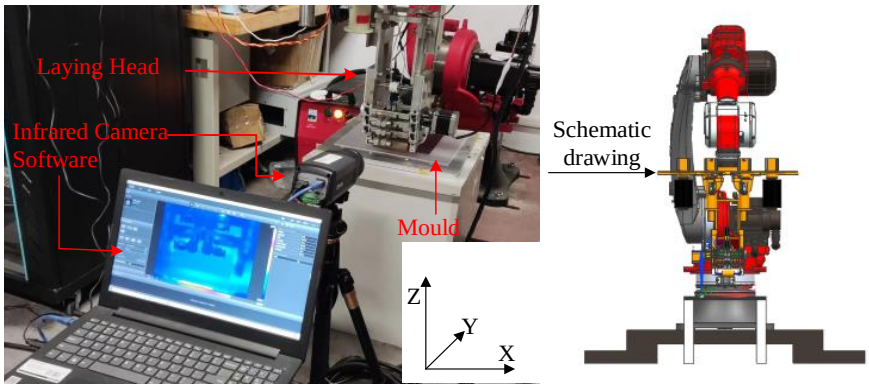

Figure 1. Layout of the thermal imaging device.

2.1.2. Experimental procedures

The purpose of monitoring the placement process is to identify and detect potential defects that may arise during the layering process. The detection system is based on two fundamental principles according to its application: edge detection, which determines the placement position and geometry, and surface detection, which identifies defects and foreign objects. Through edge detection, the system can detect the edge positions of a region and store them in the coordinate system of the robotic placement system. On the other hand, surface detection is responsible for identifying anomalies during the placement process and determining the defect coordinates related to the planned position. Both monitoring methods are based on a common principle. Notably, in the pressure points of the compaction roller and the thermographic monitoring area, there are significant temperature variations between the edge and the bundle, as well as between the normal and defective areas. When these temperature differences exceed a predetermined threshold, they are classified as edge or defect. Thus, the actual position can be approximated by comparing the planned position with the algorithm, which then determines the location and gap width. The process flow is shown in Figure 2.

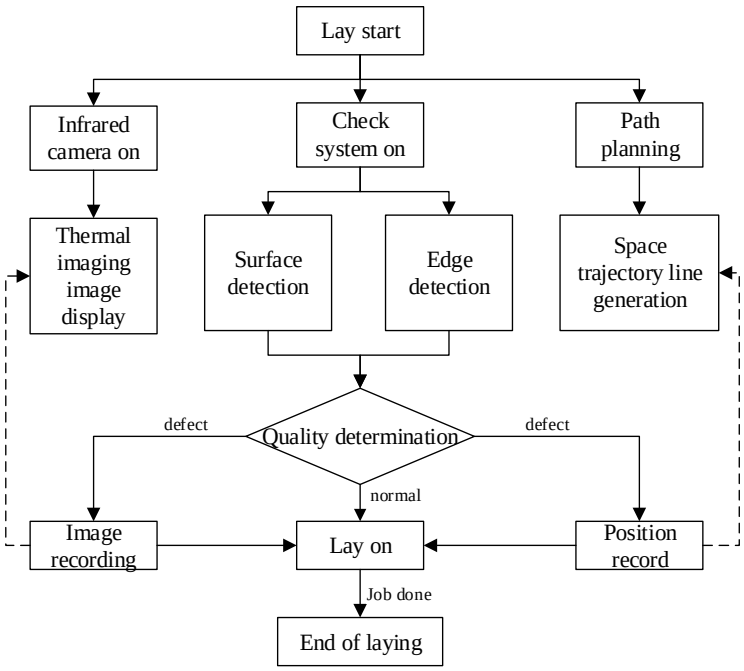

Figure 2. Defect identification and positioning flow chart.

During the automated carbon fiber layup process, a series of defects frequently occur, as shown in Figure 3. Due to structural variations, these irregular placements exhibit distinct thermal characteristics, resulting in varying rates of temperature increase under the same heating conditions. This thermal contrast is visually represented by color differences in the infrared detection system.

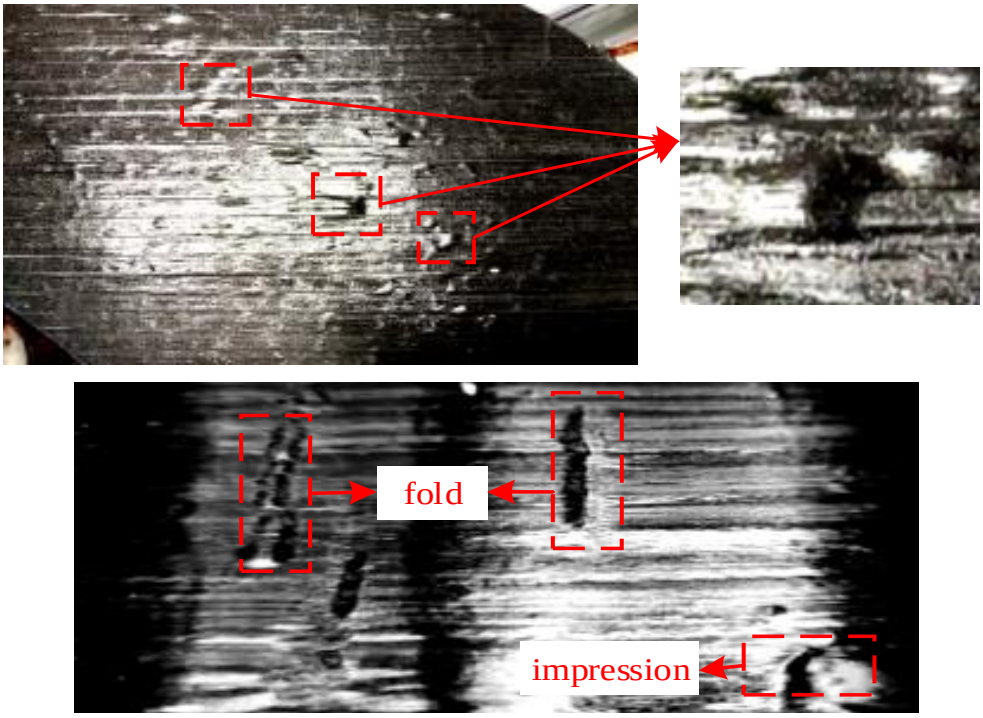

Figure 3. Common lay defect diagram.

Therefore, as shown in Figure 4, different detection regions are established for each stage of the layup process. To identify temperature irregularities such as hot spots and cold spots, the temperature values within these detection regions are compared against the uniquely dynamically generated threshold for each region.

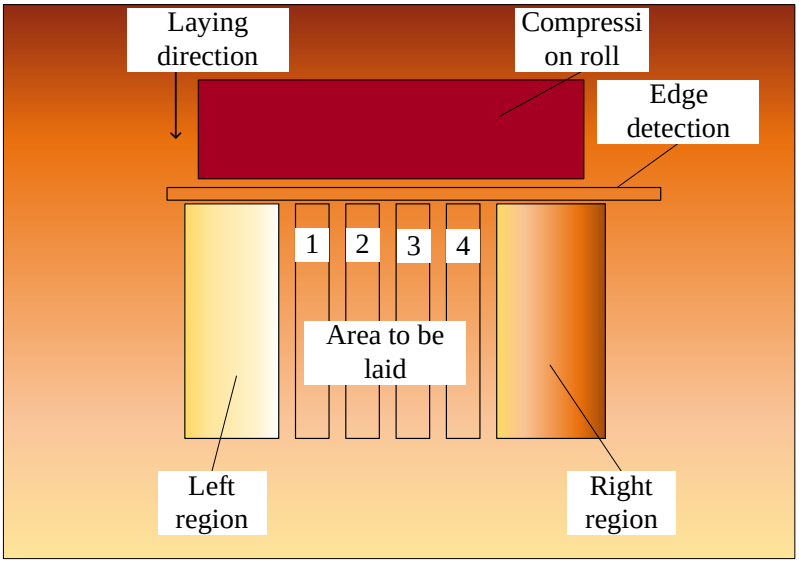

Figure 4. Thermal imaging diagram containing the area to be inspected.

The specific experimental procedures are outlined as follows:

The first step involves designing an 8-layer symmetric carbon fiber laminate using Supervisory Control and Data Acquisition (SCADA) software. As shown in Figure 5, each layer is oriented in the sequence of 0°, 90°, 45°, −45°, −45°, 45°, 90°, 0°. The length of each layer is standardized to 40 mm. The drag width is configured to 6.35 mm, the layup temperature is set to 40 °C, and the layup speed is adjusted to 40 mm/s.

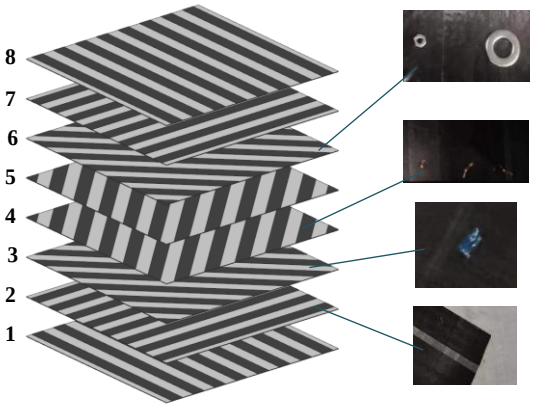

Figure 5. Placement direction and defect arrangement on each floor.

Step 2: Place corresponding defects in each layer as specified in Table 1.

Table 1. The laying angle and defect arrangement of each layer.

Floor number	1	2	3	4	5	6	7
Deflection Angle	0°	90°	45°	−45°	−45°	45°	90°
Defect	There is no	A single strand is missing	Blue plastic	Fine copper wire	There is no	Small nut gasket	There is no

2.2. Results and discussion

As shown in Figure 6, to evaluate the monitoring system, a 280 mm × 280 mm region was selected in the center of the laminate. Within this region, the carbon fiber layers are uniformly arranged, except for the presence of delamination.

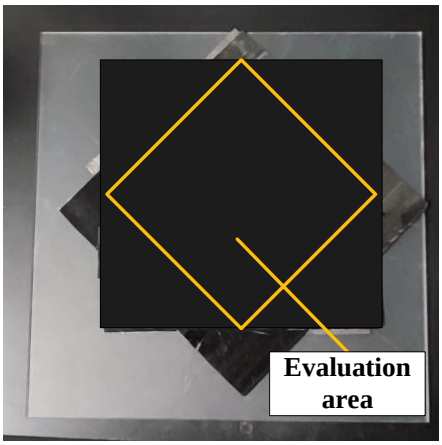

Figure 6. Experimental setup and evaluation area.

During the experiment, temperature values were sequentially recorded frame by frame from six designated points located in the left and right regions (Areas 1–4) under the same X scale. This procedure was implemented to establish a standard that describes the temperature differences and temporal temperature variations between these six regions. As shown in Figure 7, around frame 20, the temperature rise in each region at this specific location became noticeable. This phenomenon can be attributed to the passage of the compaction roller, with each point positioned directly behind the roller, leading to increased heat transfer at these six points. Temperature distribution analysis indicates that the highest temperatures are observed in Bundles 1 and 2, as these points are located at the heating center and experience less heat loss compared to Bundles 3 and 4. Bundle 2's temperature is slightly higher than that of Bundle 3, while Bundle 1's temperature is higher than Bundle 4's, and the left-side regions are warmer than the right-side regions. This difference can be explained by the fact that, in addition to the initial layup of each layer, the material already laid is typically stored in the left region, retaining the residual heat from the layup process. Moreover, the presence of these laid materials enhances the thermal insulation of the left-side regions. As a result, the temperature in the left three regions is higher than that in the right-side regions.

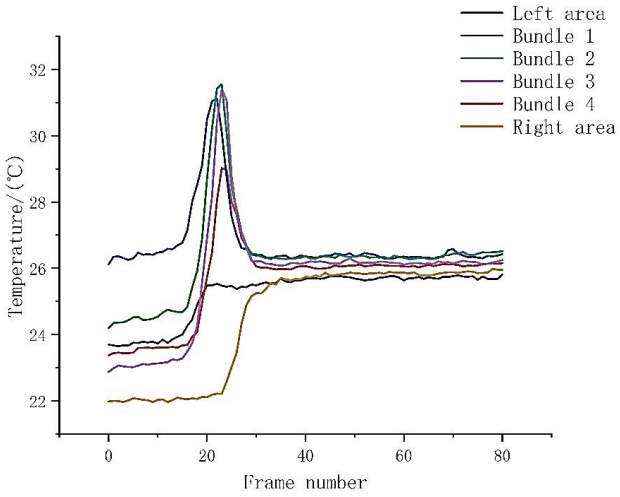

Figure 7. Temperature changes by region.

During edge detection, the temperature behind the compaction roller was selected as the target. Temperature difference data between Chain 1 and the left region, as well as between Chain 4 and the right region at the edge, were repeatedly collected and averaged for further analysis. As shown in Figure 8, compared to the subsequent layers, the edges of the first two layers exhibit lower temperatures. This is primarily due to the initial layers being positioned on the acrylic board, which has a lower heat dissipation capability, thus retaining more heat. Between the 3rd and 8th layers, the temperature difference between Bundle 1 and the left region shows a downward trend, while the temperature difference between Bundle 4 and the right region shows an upward trend. These trends are attributed to the residual heat in the left region, where the layup process has already been completed.

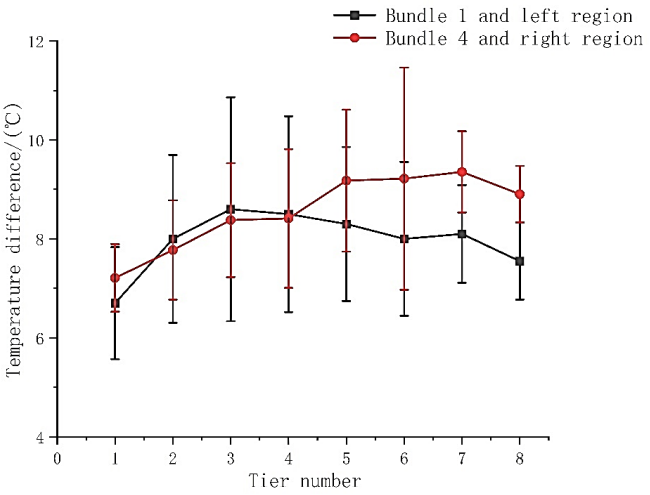

Figure 8. Temperature difference at the edge of each layer.

In the edge detection experiment, temperature sampling points are identified every 1 mm along the movement direction for each layer within the evaluation region shown in Figure 5. The infrared camera is used to measure the temperature at these designated points, and the results are plotted, as shown in Figure 6, to identify the peaks. This method is used as the evaluation standard for assessing the accuracy of edge detection.

The temperature differences shown in Figure 8 indicate that the variations in the initial two layers are relatively small, resulting in a lower edge detection rate in the actual experiment when compared to theoretical predictions. To improve the edge detection rate for the first and second layers, the threshold of the edge detection algorithm was fine-tuned, as shown in Table 2. This adjustment resulted in a detection rate of 94.3% for the outer edge of the first layer, without detecting false edges. The detection rates for the second and fourth layers were already ideal, eliminating the need for further adjustments to the threshold in subsequent layers, thus achieving satisfactory detection rates. When the layup gap was set to 0.2 mm, edge detection between single layups could not be achieved. In this setting, gaps larger than 1 mm were detectable.

Table 2. Edge detection rate of each layer.

Ply number	Left margin (100%)	Right margin (100%)	Interlayer clearance (100%)
1	99.3	94.3	8.9
2	99.6	97.5	4.1
3	100	100	1.6
4	100	98.9	2.3
5	100	100	0.8
6	100	100	1.7
7	100	100	1.3
8	100	100	0.7

As shown in Figure 9, the recognized edges are transferred from the camera coordinate system to the layup coordinate system by utilizing the position of the layup head. This conversion allows the detected edges to be plotted in the layup coordinate system. Connected edges are represented by green lines, and any identified defects are marked with red dots. In the second layer, deliberately missing individual filaments and defects located at the outer diameter edge that were not detected can be

observed. Moving to the third layer, deliberately placed blue plastic, bonding between the filaments and the compaction roller, and defects at the outer diameter edge that were not detected are visible. Similarly, in the fourth layer, deliberately placed copper wire and undetected outer diameter edge defects are visible. The sixth layer shows deliberately placed metal spacers and undetected outer diameter edge defects, while random defects in other layers are also captured by the detection system. By establishing communication between the detection system and the thermography system, the thermal imaging corresponding to the red dots in the coordinate system can be observed.

The thermography monitoring system is capable of locating the position of each individual layup within each layer, independent of the carbon fiber layup direction and the position of the previous layup. By integrating and analyzing the trajectory data, it can identify gaps between individual layups and monitor the width of these gaps. In cases where foreign objects are present near the layup path, either before or after the compaction roller, the system not only captures the temperature distribution of these objects directly using an infrared camera, but also determines their spatial coordinates. This functionality aids in monitoring the quality of the laminate throughout the carbon fiber placement process.

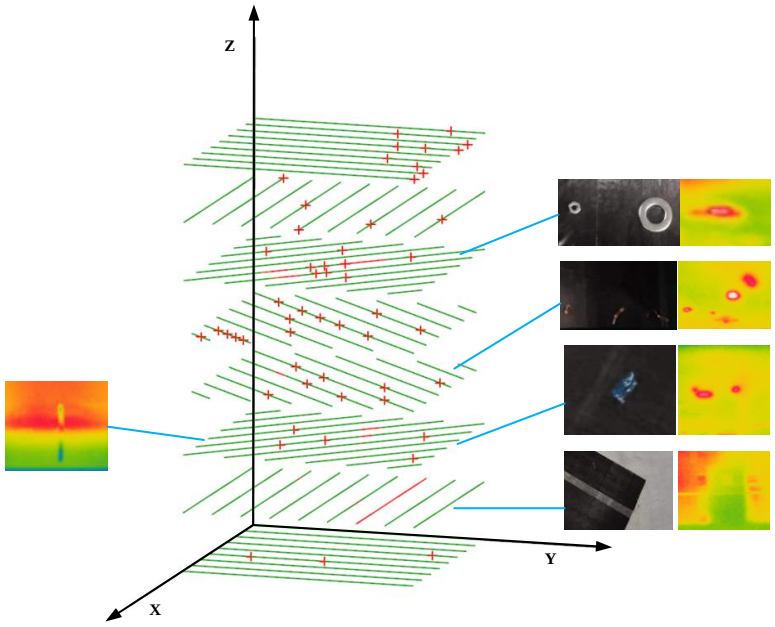

Figure 9. Monitoring of laying defects in each layer.

3. Dynamic temperature controlling methodology for defect suppression

3.1. Dynamic constant temperature control model

The current manufacturing techniques and processes ensure consistently high quality [26–27]. One aspect to be considered in that matter is the ability of the prepreg to adhere and to maintain the desired position, which is given by a certain level of tackiness. In order to maintain it in the desired position, the material laid must provide a certain level of stickiness [28]. Tack levels are formulated to guarantee that the material remains in place, or can be repositioned, if necessary, throughout the lamination process. In combination with drape, the prepreg tackiness level is of utmost importance for a successful outcome in automated technology [29]. During the automated laying process of carbon fiber, the temperature at which the carbon fiber is laid plays a crucial role in influencing various aspects such as the viscosity of

the carbon fiber prepreg, resin curing, and fiber deformation. These factors ultimately determine the structure, performance, and quality of the components being formed. Viscosity, serving as a key indicator of the prepreg's lay-up and adhesive performance, significantly impacts the bonding strength between the fiber and the matrix. The correlation between the viscosity of the surface resin of the prepreg and temperature can be mathematically described using the Arrhenius equation [30].

$$k = Ae^{\frac{E}{RT}} \tag{1}$$

In the equation: A is the characteristic viscosity (constant); E is the activation energy, R is the gas constant, T is the thermodynamic temperature.

As can be seen from the above equation, the viscosity of the resin on the surface of the prepreg diminishes as the temperature increases within a certain temperature range, indicating a direct relationship between temperature variation and viscosity within this range. Hence, maintaining dynamic temperature control during the laying process is crucial to sustain the appropriate tackiness of the fiber bundles, which is essential for the laying and forming processes of carbon fiber composites.

The relationship between the radiation intensity and the power of the infrared lamp.

$$E = \frac{P}{2\pi R\delta L} \tag{2}$$

In the above formula, E is the heat radiation intensity of the filament, unit $J/\left(m^2 \cdot s\right)$. P is the output power of the lamp, the unit is W. δ is the helical density coefficient of the lamp filament. R is the radius of the lamp. L is the length of the lamp, the unit is m.

As shown in Figure 10, the infrared heat lamp is installed on the laying head and its relative position does not change. Given the minimal and inconsequential deformation of the press roll during the laying and pressing procedures, it is reasonable to assume that the distance between the heating lamp and the heated prepreg remains relatively stable. Owing to the impact of radiation intensity and spatial orientation, heat radiation occurs within a specific area, with the surface of the region distributed in the direction of tow transmission.

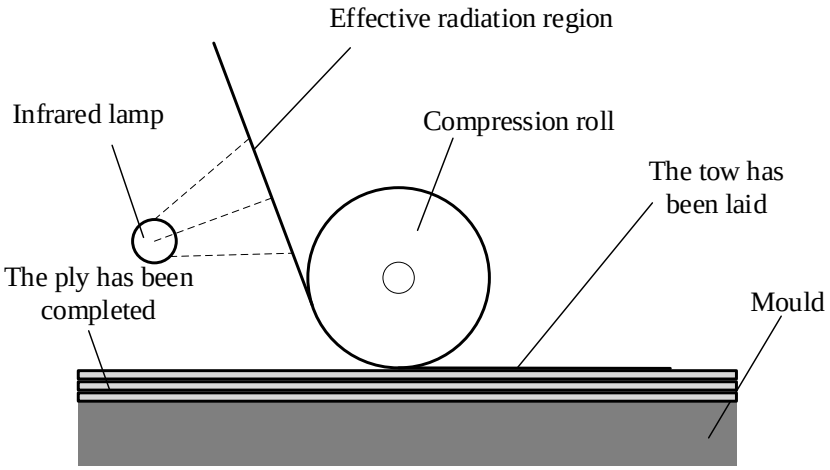

Figure 10. Schematic diagram of the heating process.

The temperature increase in the effective heating region of the carbon fiber tow can be primarily attributed to the conversion of thermal radiation emitted by the infrared heating lamp into heat energy

by the effective radiation surface. During this process, the effective radiation region receives not only to the direct radiation directly emitted by the lamp but also to the scattered indirect radiation energy from the lamp's wall that reaches the effective radiation region.

The direct radiant energy received by an effective radiating surface per unit time Q_Z it can be calculated by the following formula.

$$Q_z = \varphi_1 EA \tag{3}$$

In the above formula, φ_1 represents the percentage of radiation emitted by the filament that ultimately falls within the effective radiation region.

The indirect radiation energy received by an effective radiating surface per unit time Q_j it can be calculated by the following formula.

$$Q_j = \varphi_2 \varphi_3 \zeta EA \tag{4}$$

In the above formula, φ_2 is the percentage of radiant energy emitted by the filament that eventually falls on the wall of the lamp tube, φ_2 is the percentage of radiant energy scattered by the wall of the filament tube that eventually falls on the effective radiation region, ζ is the reflectivity of the reflection path.

Since the total radiation energy absorbed by the surface to be laid is the sum of direct radiation and indirect radiation, when the surface of the prepreg is set as a gray body, the total radiation energy absorbed in the effective radiation area per unit time Q it can be represented by the following formula.

$$Q = \lambda(Q_z + Q_j) = \lambda(\varphi_1 EA + \varphi_2 \varphi_3 \zeta EA) = \lambda(\varphi_1 + \varphi_2 \varphi_3 \zeta)P \tag{5}$$

In the above formula, λ is the absorption rate, that is, the ratio of the absorbed radiation on the surface of the tow in the effective radiation region to the total radiation, generally a constant.

Through the above analysis, the positive correlation between the absorption radiation of the effective radiation region and the power of the infrared heating lamp in unit time is established. The heat storage of the tow in unit time can be controlled by adjusting the power of the infrared heating lamp, so as to achieve temperature control. However, in the actual carbon fiber laying process, because the heating lamp moves synchronously with the laying head, the effective radiation area receives radiation action time is affected by the laying speed, so the influence of laying speed needs to be analyzed when calculating the total energy.

It is assumed that during the process of carbon fiber laying, the filament moves relative to the infrared lamp at a constant speed v, and the effective radiation region receives the thermal radiation energy from the lamp and the temperature increases accordingly. According to the law of conservation of energy, its temperature rise process can be represented by the following formula.

$$Q_a = cm\Delta T \tag{6}$$

In the above formula, Q_a is the heat absorbed during the temperature rise of the tow, and the unit is J. c is the specific heat capacity of the prepreg, in $J/(Kg \cdot ℃)$. m is the mass of the prepreg in the effective radiation area, and the unit is Kg. ΔT is the difference between the prepreg surface temperature T_1 after heating and the prepreg surface temperature T_0 before heating, in the unit of ℃.

The calculation formula of simultaneous velocity, formula (5) and formula (6).

$$\begin{cases} cm\Delta T = Q_a = Qt = \lambda(\varphi_1 + \varphi_2\varphi_3\zeta)Pt \\ L = vt \end{cases} \tag{7}$$

In the above formula, v is the wire transfer speed, the unit is $\mathrm{m/s}$. t is the time of the tow in the effective radiation area, expressed in S.

In the process of carbon fiber laying, the laying length of carbon fiber tow per unit time is equal to the transmission length of the tow, so the laying speed is equal to the transmission speed of the tow. Based on the derivation of formula (7), it can be obtained:

$$T_1 = \frac{P\lambda(\varphi_1 + \varphi_2\varphi_3\zeta)L}{cmv} + T_0 \tag{8}$$

Because φ_1, φ_2, φ_3 is a geometric factor, and during the placement process, the relative position between the infrared lamp and the placement head is unchanged, it can be identified as a constant value. And because λ, ζ, L, c, m is the fixed value. If $\kappa = \lambda(\varphi_1 + \varphi_2\varphi_3\zeta)L/cmv$ is used, the temperature rise coefficient k of the infrared lamp is also constant. Formula (7) can be converted to

$$T_1 = \kappa\frac{P}{v} + T_0 . \tag{9}$$

Formula (9) is the mathematical model of dynamic constant temperature control of carbon fiber prepreg in the automatic laying process, which shows the relative relationship between the tow temperature in the effective radiation region, the power of the infrared heating lamp and the laying speed. After the value of k is determined by experiment, when the laying temperature or laying speed is set to a fixed value, The control system can adjust another laying parameter by changing the lamp power.

3.2. Experimental results and discussion

To validate the accuracy of the aforementioned mathematical model, a verification process was carried out. The temperature measurement setup, depicted in Figure 11, comprises an infrared camera and a computer. The infrared camera is utilized to monitor temperature values and heat distribution during the laying process. As indicated in Figure 11 (b), a detection software is employed to calibrate the effective radiation area and compute the average temperature. Subsequently, the average temperature data is exported in CSV format, with the maximum value being determined as the effective radiation surface temperature for subsequent calculations.

Before commencing the experiment, carbon fiber tows are extracted from the refrigerated cabinet and left to thaw for 3 hours at room temperature (25 °C) to achieve a uniform surface temperature close to ambient conditions. The power of the infrared heating lamp is regulated through a thyristor, with a range of 50 to 250 W. The lay-up speed is managed by the robotic control system, fluctuating between 2 to 10 mm/s. Table 3 illustrates the surface temperature values of the effective radiation area at various heating powers and lay-up speeds.

The data from Table 3 were analyzed to generate the graphs depicted in Figure 12. In Figure 12 (a), it is observed that at a constant power level, the temperature decreases as the speed increases, exhibiting a strong correlation consistent with an inverse proportion function. Conversely, Figure 12 (b) demonstrates that at a constant speed, the temperature increases with a rise in power, suggesting a linear correlation.

(a)

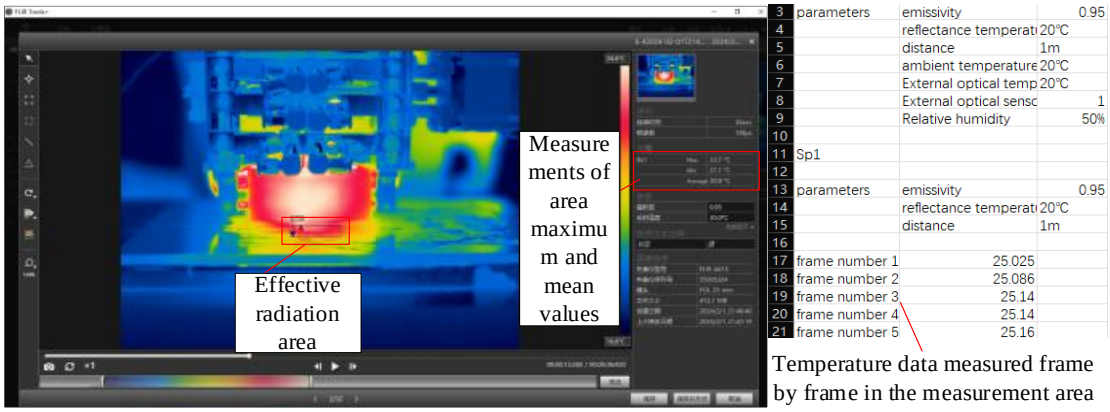

(b)

Figure 11. Temperature testing device. **(a)** Temperature monitoring equipment; **(b)** Effective radiation area temperature measurement and derived data.

Table 3. Temperature of the effective radiation area (°C) at different power and speed.

T1 (℃)	50 W	100 W	150 W	200 W	250 W
2 mm/s	35.3	46.5	57.4	67.6	74.7
4 mm/s	30.2	35.3	41.2	46.8	55.2
6 mm/s	28.2	32.5	35.4	39.7	41.7
8 mm/s	27.5	30.4	33.5	35.3	38.7
10 mm/s	26.9	29.4	31	33.4	32.4

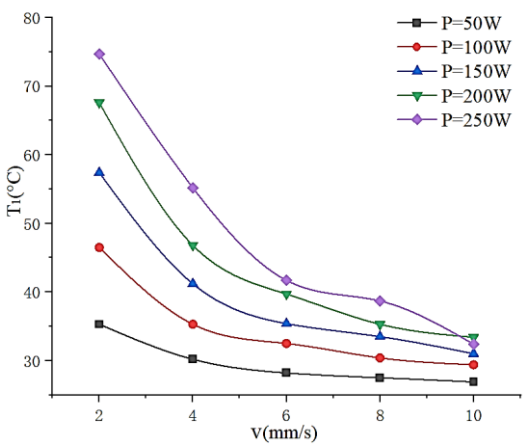

(a)

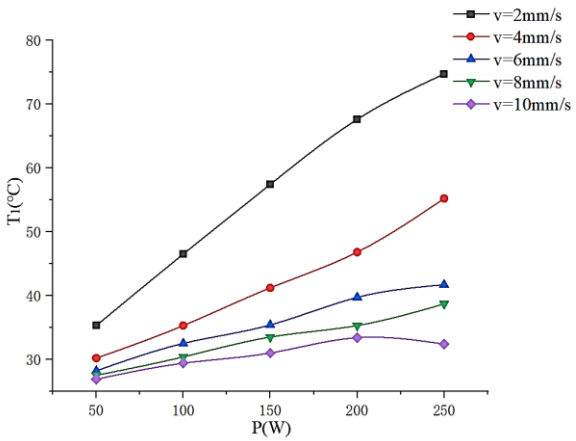

(b)

Figure 12. Image of temperature test data. **(a)** Surface temperature varies with velocity; **(b)** The surface temperature varies with power.

Given that the initial temperature of the carbon fiber tow closely approximates room temperature, it is assumed that the initial temperature of the carbon fiber tow $T_0 = 25°C$ calculated to determine the temperature difference under varying powers and speeds. The results are presented in Table 4.

Table 4. Temperature difference at different power and speed (°C).

△T (°C)	50 W	100 W	150 W	200 W	250 W
2 mm/s	10.3	21.5	32.4	42.6	49.7
4 mm/s	5.2	10.3	16.2	21.8	30.2
6 mm/s	3.2	7.5	10.4	14.7	16.7
8 mm/s	2.5	5.4	8.5	10.3	13.7
10 mm/s	1.9	4.4	6	8.4	10.4

Based on the above analysis, the objective functions are an inverse proportional function and a linear function, respectively. The fitted function curves are shown in Figure 13. The data points are evenly distributed on both sides of the graph, confirming the accuracy of the fitting results. By using the fitted function, the infrared lamp temperature rise coefficient $k = 0.428$ is determined, indicating that Equation (12) can accurately describe the temperature variation during the layup process.

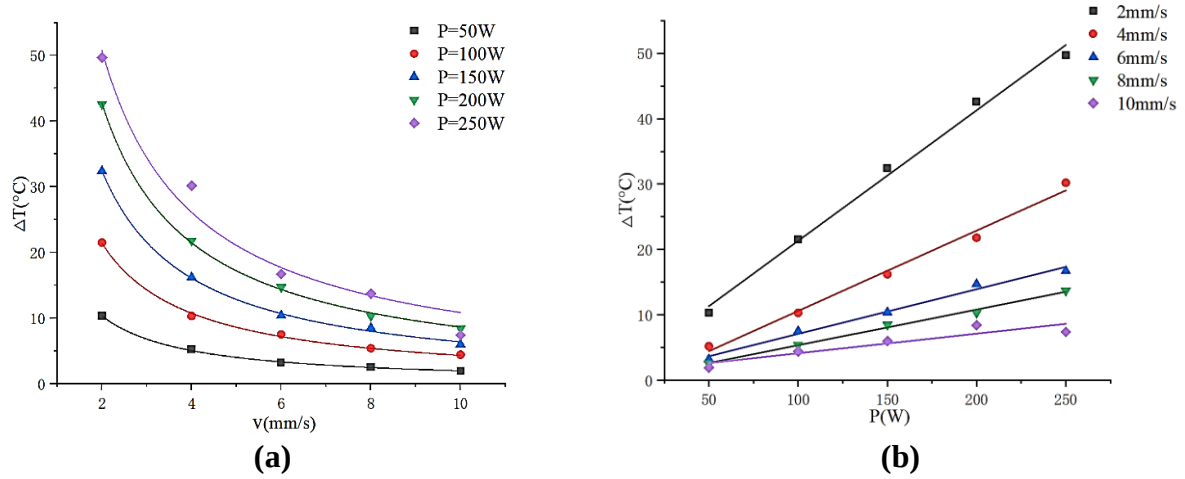

Figure 13. Image of temperature difference test data. **(a)** Surface temperature difference varies with velocity; **(b)** The surface temperature difference varies with power.

Based on the aforementioned temperature control model, the layup effect of the carbon fiber tow is shown in Figure 14. The overall result is relatively smooth, with fewer bubbles caused by improper laying temperature, and interlayer separation due to uneven compaction is not significant.

Figure 14. The carbon fiber layup effect diagram.

The experimental verification ultimately confirmed the accuracy of the established infrared lamp heating model, providing a mathematical framework for temperature regulation during the layup process. Within the temperature control protocol, the heating power of the infrared lamp is modulated through a silicon-controlled rectifier (SCR) power controller. This ensures the stability of the surface temperature within the effective radiation area of the filament at different layup speeds, thereby reducing layup defects caused by temperature fluctuations.

4. Conclusion

The designed thermal imaging detection system can efficiently identify and locate defects during the carbon fiber laying process, with a detection rate of up to 94.3%. At the same time, the established dynamic temperature control model is effective, and the experimental results of the surface temperature difference variation with speed and power align with the model. The temperature rise coefficient can be considered constant. In the automated laying process, the control system can optimize the laying parameters by adjusting the lamp tube power, reducing defects caused by temperature variations.

(1) Utilizing the developed thermal imaging detection system enables the identification and localization of defects that may occur during the carbon fiber laying process. By setting a specific threshold, it was observed that the minimum edge detection rate on both sides within a single layer reached 94.3%, with interlayer gaps measuring less than 10%. Defects manually set are clearly visible in the coordinate system, thus indicating the efficacy of the detection system.

(2) The established dynamic thermostatic model for the carbon fiber laying process has proven to be effective. Through experiments conducted to analyze surface temperature variations in response to changes in speed and power, the derived functions closely align with the established mathematical model. It can be inferred that, under these specific conditions, the calculated coefficient for the temperature rise of the infrared lamp remains constant, and $k = 0.428$. During the automated layup process, when the layup speed is set to a fixed value, the control system can adjust other layup parameters by varying the lamp power, in order to reduce layup defects caused by temperature fluctuations.

Authors' contribution

Conceptualization, Yixuan Xie, Zhiqiang Liu, Yinqi Li and Yueyue Zong; methodology, Yixuan Xie, Zhiqiang Liu and Yinqi; software, Yixuan Xie and Yinqi Li; validation, Yixuan Xie and Yueyue Zong; formal analysis, Yixuan Xie; investigation, Yixuan Xie; resources, Yixuan Xie; data curation, Yixuan Xie, Yinqi Li and Yueyue Zong; writing—original draft preparation, Yixuan Xie, Yinqi Li and Yueyue Zong; writing—review and editing, Yixuan Xie, Zhiqiang Liu, Yinqi Li and Yueyue Zong; visualization, Yixuan Xie and Yinqi; supervision, Zhiqiang Liu; project administration, Zhiqiang Liu; All authors have read and agreed to the published version of the manuscript.

Conflicts of interests

The authors declare that no funds, grants, or other support were received during the preparation of this

manuscript. The authors have no relevant financial or non-financial interests to disclose.

Reference

[1] Yang D, Dong S, Hong C, Zhang X. Preparation, modification, and coating for carbon-bonded carbon fiber composites: a review. *Ceram. Int. 2022*, 48(11):14935–58.

[2] Nsengiyumva W, Zhong S, Lin J, Zhang Q, Zhong J. Advances, limitations and prospects of nondestructive testing and evaluation of thick composites and sandwich structures: A state-of-the-art review. *Compos. Struct.* 2021, 256:112951.

[3] Stawiarski A. The nondestructive evaluation of the GFRP composite plate with an elliptical hole under fatigue loading conditions, *Mech. Syst. Signal Process.* 2018, 112:31–43.

[4] Rocha H, Semprimoschnig C, Nunes JP. Sensors for process and structural health monitoring of aerospace composites: A review. *Eng. Struct.* 2021, 237:112231.

[5] Zhang J, Yao D, Wang R, Xiao X. Vibro-acoustic modelling of high-speed train composite floor and contribution analysis of its constituent materials. *Compos. Struct.* 2021, 256:113049.

[6] Huang L, Zeng L, Lin J, Luo Z. An improved time reversal method for diagnostics of composite plates using lamb waves. *Compos. Struct.* 2018, 190 :10–19.

[7] Ren Y, Qiu L, Yuan S, Fang F. Gaussian mixture model and delay-and-sum based 4D imaging of damage in aircraft composite structures under time-varying conditions. *Mech. Syst. Signal Process.* 2020, 135:106390.

[8] Gholizadeh S. A review of non-destructive testing methods of composite materials. *Procedia Struct. Integrity* 2016, 1:50–57.

[9] Duchene P, Chaki S, Ayadi A, Krawczak P. A review of non-destructive techniques used for mechanical damage assessment in polymer composites. *J. Mater. Sci.* 2018, 53(11):7915–7938.

[10] Memmolo V, Monaco E, Boffa ND, Maio L, Ricci F. Guided wave propagation and scattering for structural health monitoring of stiffened composites. *Compos. Struct.* 2018, 184:568–580.

[11] Cui R, Wiggers de Souza C, Katko BJ, Lanza di Scalea F, Kim H. Non-destructive damage localization in built-up composite aerospace structures by ultrasonic guided-wave multiple-output scanning. *Compos. Struct.* 2022, 292:115670.

[12] Wang B, Zhong S, Lee TL, Fancey KS, Mi J. Non-destructive testing and evaluation of composite materials/structures: A state-of-the-art review. *Adv. Mech. Eng.* 2020, 12(4):1–28.

[13] Broberg P. Surface crack detection in welds using thermography. *NDT&E Int.* 2013, 57:69–73.

[14] Keo SA, Brachelet F, Breaban F, Defer D. Defect detection in CFRP by infrared thermography with CO2 Laser excitation compared to conventional lock-in infrared thermography. *Compos. Part B Eng.* 2015, 69:1–5.

[15] Schlichting J, Maierhofer C, Kreutzbruck M. Crack sizing by laser excited ther-mography. *NDT&E Int.* 2012, 45:133–40.

[16] Roemer J, Uhl T, Pieczonka Ł. Laser spot thermography for crack detection in aluminum structures. In *7th International Symposium on NDT in Aerospace—We.5. A.5*, Bremen, Germany, November 16–18, 2015.

[17] Pech-May NW, Oleaga A, Mendioroz A, Salazar A. Fast characterization of the width of vertical cracks using pulsed laser spot infrared thermography. *J. Nondestr. Eval.* 2016, 35:22.

[18] Fedala Y, Streza M, Sepulveda F, Roger JP, Tessier G, *et al*. Infrared Lock-in Thermography Crack Localization on Metallic Surfaces for Industrial Diagnosis. *J. Nondestr. Eval.* 2014, 33(3):335–341.
[19] Lukaszewicz DHJA. *Optimisation of high-speed automated layup of thermoset carbon-fibre preimpregnates*. Bristol: University of Bristol, 2011.
[20] Hulcher AB, Banks III WI, Pipes RB, Tiwari SN, Cano RJ, *et al.* Automated fiber placement of PEEK/IM7 composites with film interleaf layers. *NASA Report*. 2001, 46(1):1998–2012.
[21] Aized T, Shirinzadeh B. Robotic fiber placement process analysis and optimization using response surface method. *Int. J. Adv. Manuf. Technol.* 2011, 55(1):393–404.
[22] Mehrabian M, Boukhili R. 3D-DIC strain field measurements in bolted and hybrid bolted-bonded joints of woven carbon-epoxy composites. *Compos. Part B Eng.* 2021, 218:108875.
[23] Doshvarpassand S, Wu C, Wang X. An overview of corrosion defect characterization using active infrared thermography. *Infrared Phys. Technol.* 2019, 96:366–389.
[24] He Y, Deng B, Wang H, Cheng L, Zhou K, *et al.* Infrared machine vision and infrared thermography with deep learning: A review. *Infrared Phys. Technol.* 2021, 116:103754.
[25] Rippa M, Pagliarulo V, Lanzillo A, Grilli M, Fatigati G, *et al.* Active thermography for non-invasive inspection of an artwork on poplar panel: Novel approach using principal component thermography and absolute thermal contrast. *J. Nondestr. Eval.* 2021, 40:21.
[26] Nelson ES, Reddy DR. *Green aviation reduction of environmental impact through aircraft technology and alternative fuels*. Florida: CRC Press, 2020.
[27] A Gardziella, LA. Pilato, A Knop. *Phenolic Resins: Chemistry, Applications, Standardization, Safety and Ecology*. Berlin: Springer, 2000.
[28] Smith RP, Qureshi Z, Scaife RJ, El-Dessouky HM. Limitations of processing carbon fibre reinforced plastic/polymer material using automated fibre placement technology. *J. Reinf. Plast. Compos.* 2016, 35(21):1527–1542.
[29] Budelmann D, Schmidt C, Meiners D. Prepreg tack: A review of mechanisms, measurement, and manufacturing implication. *Polym. Compos.* 2020, 41:3440–3458.
[30] Li Y, Zhu F, Xiao J. The affection of additions component on viscosity of up resin. *Hi-Tech Fiber & Appl.* 2002, 27(3):28–30.